A bright, high rotation-measure FRB that skewers the M33 halo

Liam Connor[1,2], Joeri van Leeuwen[2,1], L. C. Oostrum[2,1], E. Petroff[1,3], Yogesh Maan[2], J. J. Attema[4], J. E. Bast[2], O. M. Boersma[1,2], H. Dénes[2], D. W. Gardenier[2,1], J. E. Hargreaves[2], E. Kooistra[2], I. Pastor-Marazuela[1,2], R. Schulz[2], A. Sclocco[4], R. Smits[2], S. M. Straal[5,6], D. van der Schuur[2], Dany Vohl[2], E. A. K. Adams[2,7], B. Adebahr[8], W. J. G. de Blok[2,9,7], W. A. van Cappellen[2], A. H. W. M. Coolen[2], S. Damstra[2], G. N. J. van Diepen[2], B. S. Frank[10,9], K. M. Hess[2,7], B. Hut[2], G. Marcel Loose[2], D. M. Lucero[11], Á. Mika[2], V. A. Moss[12,13,2], H. Mulder[2], T. A. Oosterloo[2,7], M. Ruiter[2], N. J. Vermaas[2], S. J. Wijnholds[2], J. Ziemke[2,14]

[1] *Anton Pannekoek Institute, University of Amsterdam, Postbus 94249, 1090 GE Amsterdam, The Netherlands*
[2] *ASTRON, the Netherlands Institute for Radio Astronomy, Oude Hoogeveesedijk 4,7991 PD Dwingeloo, The Netherlands*
[3] *Veni Fellow*
[4] *Netherlands eScience Center, Science Park 140, 1098 XG, Amsterdam, The Netherlands*
[5] *NYU Abu Dhabi, PO Box 129188, Abu Dhabi, United Arab Emirates*
[6] *Center for Astro, Particle, and Planetary Physics (CAP^3), NYU Abu Dhabi, PO Box 129188, Abu Dhabi, United Arab Emirates*
[7] *Kapteyn Astronomical Institute, PO Box 800, 9700 AV Groningen, The Netherlands*
[8] *Astronomisches Institut der Ruhr-Universität Bochum (AIRUB), Universitätsstrasse 150, 44780 Bochum, Germany*
[9] *Dept. of Astronomy, Univ. of Cape Town, Private Bag X3, Rondebosch 7701, South Africa*
[10] *South African Radio Astronomy Observatory (SARAO), 2 Fir Street, Observatory, 7925, South Africa*
[11] *Department of Physics, Virginia Polytechnic Institute and State University, 50 West Campus Drive, Blacksburg, VA 24061, USA*
[12] *CSIRO Astronomy and Space Science, Australia Telescope National Facility, PO Box 76, Epping NSW 1710, Australia*
[13] *Sydney Institute for Astronomy, School of Physics, University of Sydney, Sydney, New South Wales 2006, Australia*
[14] *Rijksuniversiteit Groningen Center for Information Technology, P.O. Box 11044, 9700 CA Groningen, the Netherlands*

Accepted XX YY ZZZZ

ABSTRACT

We report the detection of a bright fast radio burst, FRB 191108, with Apertif on the Westerbork Synthesis Radio Telescope (WSRT). The interferometer allows us to localise the FRB to a narrow $5'' \times 7'$ ellipse by employing both multibeam information within the Apertif phased-array feed (PAF) beam pattern, and across different tied-array beams. The resulting sight line passes close to Local Group galaxy M33, with an impact parameter of only 18 kpc with respect to the core. It also traverses the much larger circumgalactic medium of M31, the Andromeda Galaxy. We find that the shared plasma of the Local Group galaxies could contribute ~10% of its dispersion measure of 588 pc cm^{-3}, but not detectable scintillation, temporal scattering, or significant Faraday rotation for this FRB. FRB 191108 has a Faraday Rotation Measure of 474±3 rad m^{-2}, too large to be explained by either the Milky Way or the intergalactic medium. This indicates a dense local magneto-ionic environment in the source host galaxy—as has been argued for other FRBs. We found no accompanying persistent radio sources in the Apertif imaging survey data.

Key words: fast radio bursts – observation – instrumentation

1 INTRODUCTION

Fast radio bursts (FRBs) are extragalactic radio pulses, of which approximately 110 have been discovered to date (Lorimer et al. 2007; Petroff et al. 2016). They are short duration (μs–ms), bright (0.01–100 Jy peak flux density), highly dispersed, and relatively common ($\sim 10^3$ sky^{-1} day^{-1} above 1 Jy; Cordes & Chatterjee 2019; Petroff et al. 2019). The most pressing questions in FRB science fall into two broad categories: What causes these mysterious bursts? And, how can they be put to use?

In the former class of questions, significant progress has been made in the past several years. A subset of FRBs has been found to repeat, first the Arecibo-discovered FRB 121102 (Spitler et al. 2014, 2016). Eighteen repeaters have been detected with the Canadian Hydrogen Intensity Mapping Experiment (CHIME) (CHIME/FRB Collaboration et al. 2019b,c; Fonseca et al. 2020) as well as one from ASKAP (Kumar et al. 2019). It is still unclear if the sources that have not been seen to repeat are of a distinct class of once-off events, or if their repetition statistics (rate, temporal clustering, luminosity function, etc.) are such that they are difficult to detect more than once with most telescopes (e.g. Kumar et al. 2019). Real-time arcsecond localisation has allowed for host galaxy identifications, shedding light on the variety of galaxies in which FRBs reside (Bannister et al. 2019; Ravi et al. 2019). Very-long-baseline interferometry (VLBI) follow up of repeating FRBs has provided milliarcsecond localisation, which has been essential in understanding the nearby progenitor environment (Marcote et al. 2017; Chatterjee et al. 2017; Tendulkar et al. 2017; Bassa et al. 2017; Michilli et al. 2018; Marcote et al. 2020).

In the FRB applications category, the theoretical proposals that have been put forward range from intergalactic medium (IGM) and circumgalactic medium (CGM) studies (McQuinn 2014; Prochaska & Zheng 2019; Vedantham & Phinney 2019), to gravitational lensing (Muñoz et al. 2016; Eichler 2017) and cosmology (Walters et al. 2018). Recently, progress has been made in putting such proposals into practice (Ravi et al. 2016; Prochaska et al. 2019).

In this paper we report the detection of FRB 191108 with the Apertif Radio Transient System (ARTS) on the Westerbork Synthesis Radio Telescope (WSRT). This source has a Faraday Rotation Measure RM=474±3 rad m^{-2}, which is an order of magnitude larger than the expected Galactic and IGM contributions. It also passes through the halo of Local Group galaxy M33 (The Triangulum Galaxy) with a best-fit impact parameter of just 18 kpc. The M33 halo is embedded in the much-larger galactic halo of M31 (The Andromeda Galaxy), which we expect to also impact the propagation of the pulse. In Sect. 2 we briefly describe the discovery pipeline. We present the burst discovery and localization efforts in Sect. 3, and discuss rotation measure and repetition constraints in Sect. 4 and conclude in Sect. 5.

2 ARTS PIPELINE

The Apertif Radio Transient System (ARTS) searches for radio pulses using ten 25-m dishes of the WSRT equipped with the new Apertif phased array feeds (PAFs; Oosterloo et al. 2010; Adams & van Leeuwen 2019). While a full description of ARTS is provided in van Leeuwen et al. (2020), we highlight a number of relevant features below.

For the real-time FRB search, we beamform the dipoles in each of the PAFs to produce 40 voltage ‘compound beams’ (CBs) with 300 MHz of bandwidth centered on a radio frequency of 1370 MHz. This is done at each dish. The compound beams are next further beamformed in firmware across the East-West array to create 12 tied-array beams (TABs) per compound beam, out of which we generate Stokes I, Q, U, and V data-streams at 81.92 µs and 195 kHz time and frequency resolution (van Leeuwen 2014). As the fractional bandwidth of Apertif is high, ∼ 0.2, the TABs must be recombined in frequency to produce ‘synthesised beams’ (SBs). A synthesised beam points in the same direction across the 300 MHz band, which is not true of a TAB. An overview of this hierarchical beamforming is provided in Maan & van Leeuwen (2017). In total, 71 synthesised beams are formed per compound beam, which span the full primary

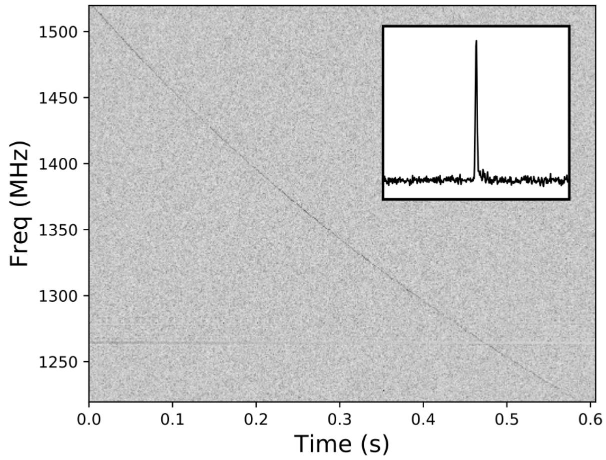

Figure 1: The dispersed dynamic spectrum of FRB 191108 across the ARTS observing bandwidth, and the dedispersed and frequency-averaged pulse profile for 30 ms of data (inset). The dynamic spectrum has been bandpass corrected and median subtracted, but not RFI cleaned. It is has been binned down to 0.82 ms time resolution with 0.78 MHz frequency channels.

beam field of view (FoV) of ∼ 0.23 deg^2. The full 40-compound-beam PAF has a FoV of roughly 9 deg^2. The total 2840 Stokes I Synthesized Beams are then searched in real time by our single-pulse search software `AMBER`[1] (Sclocco et al. 2014, 2016, 2020), which runs on a dedicated 40-node graphics processing unit (GPU) computing cluster at the WSRT site. Data post-processing is handled by Data Analysis of Real-time Candidates from the Apertif Radio Transient System (DARC ARTS[2]). Raw candidates are clustered in dispersion measure (DM), time, pulse width, and beam number; and then sent to a machine learning classifier which assigns a probability of the candidate being a true FRB (Connor & van Leeuwen 2018). While Stokes I data is always written to filterbank files on disk, the buffered Stokes Q, U, and V data are only saved if `AMBER` identifies a candidate with a total duration <10 ms, a signal-to-noise ratio (S/N hereafter) greater than 10, and a DM more than 20% larger than the predicted value along the line of sight from the YMW16 electron density model (Yao et al. 2017).

3 RESULTS

FRB 191108 was detected in three compound beams, at solar system barycentric UTC 19:48:50.240. The discovery DM was 588 pc cm^{-3}. Fig. 1 shows the dynamic spectrum of the dispersed pulse as well as the dedispersed pulse profile. The maximum S/N from the real-time detection was 60 in compound beam 21 (see Fig. 3) and our machine learning classifier assigned a probability of > 99.9% of it being a real transient (Connor & van Leeuwen 2018). The `AMBER` detection triggered a dump of the full-Stokes data, allowing us to analyse the polarisation properties of the burst.

[1] https://github.com/AA-ALERT/AMBER
[2] https://github.com/loostrum/darc

3.1 Polarisation properties

FRB 191108 was measured to be roughly 50% linearly polarised and $\leq 13\%$ circularly polarised. It was found to have an RM of $+474\pm3$ rad m^{-2}. The best-fit RM was obtained by applying a linear least squares fit to position angle (PA) as a function of wavelength squared. The sign was determined by verifying that the Crab pulsar had an RM of -43 rad m^{-2} during an observation the same day.

Both bandpass calibration and polarisation calibration were done using 3C286, a standard calibrator source, which is known to have very little circular polarisation. We treat the Stokes V value as an upper limit because of uncertainty in the polarisation calibration procedure. 3C286 was observed in the same compound beam as the FRB, but it was observed in the central TAB, where leakage is expected to be minimised. FRB 191108 was found in synthesised beam number 37, which is a linear combination of non-central TABs. That synthesised beam may have slightly different leakage properties than the central TAB, and these will be better quantified as the system is further calibrated. From the 3C286 on/off observation, we solved for a single phase in each down-channelised frequency channel, knowing that the complex XY correlation ought to be purely real if Stokes V is zero. We verified that the polarisation calibration solution agreed with a different method that used the FRB itself, which separated the component of $\mathbb{I}m\{XY\}$ that varies with λ^2 from that which does not, since Stokes V should not exhibit Faraday rotation. Fortunately, the polarisation rotation does not vary with parallactic angle on Westerbork data, as the dishes are on equatorial mounts. Thus, differences in hour angle between the two observations have no influence. Still, it is possible that the calibration solution is sufficiently different between TABs and synthesised beams that the observed 13 % circular polarisation is spurious. Fortunately, Faraday rotation is robust against uncertainty in the polarisation calibration solution, because it is difficult to mimic a rotation in the Q/U plane that is sinusoidal in λ^2. Hence, we are confident in the reported value of the rotation measure (RM).

We see no evidence of a swing in the PA across the pulse. FRB 121102 was also found to have a flat polarisation PA (Michilli et al. 2018; Gajjar et al. 2018; Hessels et al. 2019), as was FRB 180916.J0158+65 (known as R3; CHIME/FRB Collaboration et al. 2019c). This is in contrast to many pulsars; and it may have interesting implications for FRB emission mechanisms. In our case, however, the flat PA may be instrumental. While the true PA could be flat across the pulse like previous FRBs, the intrinsic width of FRB 191108 is temporally unresolved, meaning any swing in the polarisation PA is unobservable; the apparent flat PA across the pulse is the time-averaged angle of the true pulse. This can lead to depolarisation, because coarse temporal sampling and intra-channel dispersion effectively z add linear-polarisation vectors across the pulse that may point in different directions. The depolarisation fraction is,

$$f_{\mathrm{depol}}\left(\Delta\theta\right) = 1 - \cos\left(\Delta\theta/2\right) \tag{1}$$

Here, $\Delta\theta$ is the PA change across the pulse in radians. Since we observe the FRB to have $\sim 50\%$ linear polarisation, the true pulse must be at least as polarised and its $\Delta\theta$ cannot be greater than $\sim 120\,^\circ$. It is possible that FRB 191108 and other temporally-smeared FRBs with moderate polarisation fractions have higher intrinsic polarisations than inferred.

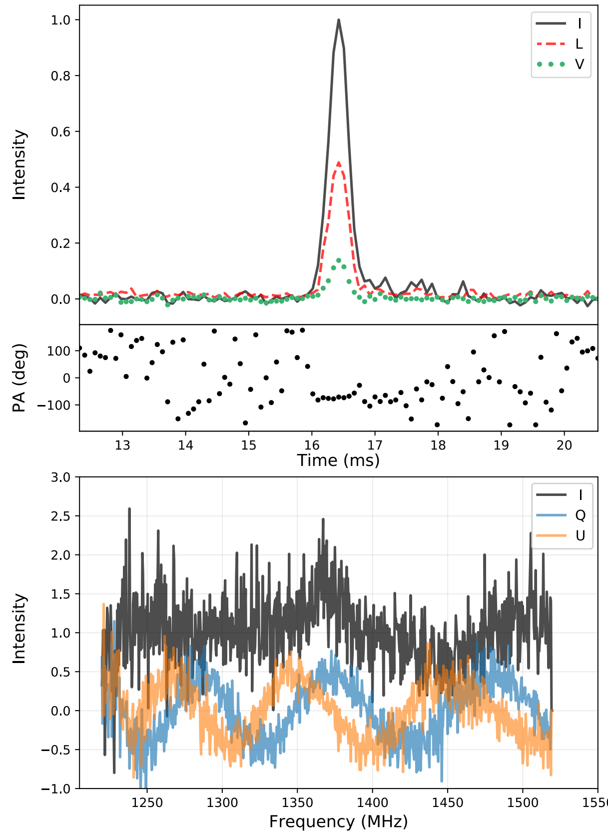

Figure 2: The measured polarisation properties of FRB 191108. The top panel shows the frequency-averaged pulse profiles after correcting for Faraday rotation in total intensity, I, linear polarisation, L, and circular polarisation, V. The middle panel shows a flat PA across the pulse, which could be intrinsic or due to depolarisation, as the true FRB width is temporally unresolved. The bottom panel shows the band-pass corrected frequency spectrum, as well as the Faraday-rotated Stokes Q and U. The best fit RM is 474 ± 3 rad m^{-2}.

3.2 Localisation

By combining multibeam information from the 40 overlapping compound beams (CBs) in a PAF, with the interferometric information contained in the TABs and synthesised beams (SBs), Apertif can achieve a theoretical localisation region of,

$$\Omega \approx \frac{30''}{S/N} \times \frac{30'}{S/N}, \tag{2}$$

although in practice this will depend on how well we know our beamshapes. In order to localise FRB 191108, we first need to obtain the S/N of the burst in each SB. The FRB was initially detected in two neighbouring compound beams, with the highest S/N in CB 21. Using the post-detection optimised DM and timestamp, we measure the S/N of the burst in all SBs of CB 21 and the ones surrounding it. Using a S/N threshold of 8, the FRB was detected in CBs 15, 21, and 22, across a total of 48 SBs. The highest S/N was 103 in SB 37 of CB 21 (hereafter the reference beam).

We create a model of the Apertif beam pattern assuming a Gaussian primary beam pattern for each compound beam, with a half-power width of 36.3′ at 1370 MHz. Each CB is then scaled using the system-equivalent flux density measured for each CB determined from a drift scan of calibrator source 3C48. Defining a grid of $40' \times 40'$ with a resolution of $1''$ centered on CB 21, we generate the TAB response of the 8 equidistant WSRT dishes across this grid and recombine these across frequency into 71 SBs per CB. The SBs are integrated across frequency, assuming a flat spectral index. The model is then scaled to the model of the reference beam, resulting in a prediction of the S/N ratio between each SB and the reference beam.

Next, we calculate the χ^2 statistic at each grid point. For SBs without a detection, we only include points where the modelled S/N is above the detection threshold and use the S/N threshold in place of the observed S/N. A 90% confidence region is derived from $\Delta\chi^2$ values using the theoretical conversion from confidence level to $\Delta\chi^2$. The localisation method has been verified using multi-beam detections of giant pulses from the Crab pulsar and single pulses from PSR J0528+2200, also in CB 21. A more accurate determination of the confidence region based on several pulsar observations is in progress.

The final derived 90% confidence region is shown in Fig. 3. The best-fit position (J2000) corresponds to RA=01:33:47, Dec=+31:51:30. The error ellipse has a semi-major axis of $3.5\,'$ and a semi-minor axis of $2.5\,''$, with a position angle of $19.5\,^\circ$ East of North. The FRB is localised to a region $1.20 \pm 0.05\,^\circ$ from the core of Local Group galaxy M33. The localisation solid angle of approximately 2100 square arcseconds (90 % confidence) is too large to unambiguously identify a host galaxy associated with the FRB, even if the DM/z relation is to be trusted and utilised (Eftekhari & Berger 2017). However, as we discuss in Sect. 4.2, if FRB 191108 is found to repeat and is detected at a different parallactic angle, we will achieve $\sim$ arcsecond localisation in both directions because the TABs will be at a different position angle on the sky.

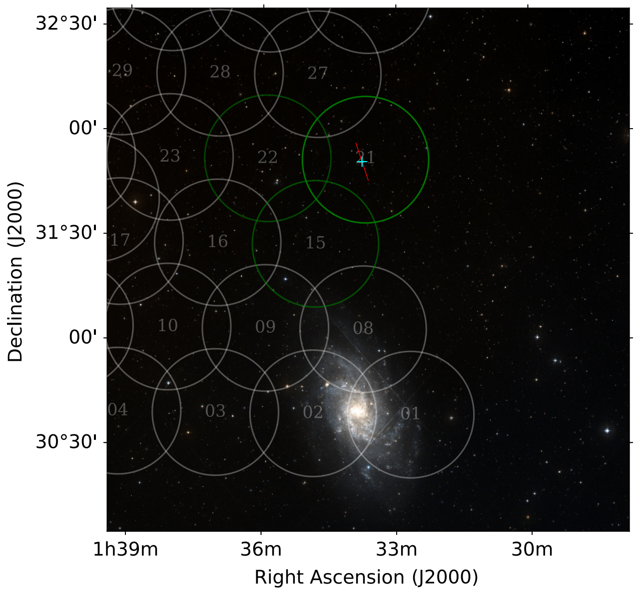

Figure 3: The localisation region of FRB 191108. The compound beams at 1370 MHz are shown in white (non-detection) and green (detection, with circle opacity in proportion to S/N). The best-fit location is shown with a blue cross. The red, elongated and very narrow area around the cross indicates the 90% confidence level localisation area. The galaxy near the bottom of the figure is M33, which is $1.20 \pm 0.05\,^\circ$ from the location of the FRB. Background image from the Sloan Digital Sky Survey (SDSS; York et al. 2000).

3.2.1 *Apertif continuum survey & radio counterpart*

We have searched for a persistent radio source associated with FRB 191108 in continuum images from the Apertif imaging surveys. The mosaic in Fig. 4 is a combination of 31 compound beams from two survey pointings (191010042 and 191209026) which overlap around the localisation region. The continuum images for the mosaic were made using the top 150 MHz of the Apertif imaging band (1280–1430 MHz). The mosaic covers $\sim 9\,\mathrm{deg}^2$ and M33 can be seen in the bottom half of the map. We did not find anything within the localisation error region above $5\,\sigma$ at 71 μJy root mean square noise.

Radio point sources have a lower on-sky density than faint optical galaxies, which decreases the probability of chance spatial coincidence and relaxes the localisation requirements for radio counterparts (Eftekhari et al. 2018). The persistent radio source associated with FRB 121102 was roughly 200 μJy at $z \approx 0.2$ at 1 GHz (Chatterjee et al. 2017), meaning we could have detected an equivalent nebula above $3\,\sigma$ if FRB 191108 were at the same distance as FRB 121102. This is more nearby than the maximum redshift implied by the extragalactic DM of FRB 191108, which is $z \approx 0.52$. Therefore, the host-galaxy ISM or the dense magnetised plasma contributing to the RM of the FRB would need to contribute significant DM in order for us to detect a persistent source similar to the one associated with FRB 121102. This is not implausible. Using the same Galactic halo modelling and DM/z relation employed in this paper, the extragalactic DM of FRB 121102 implies a redshift that is 60% larger than the known value of its host galaxy. The Galactic center magnetar, PSR J1745−2900, is both strongly Faraday rotated (RM$\approx 7 \times 10^4\,\mathrm{rad\,m^{-2}}$) and dispersed (DM$\approx$1780 $\mathrm{pc\,cm^{-3}}$) near to the source, which would make it seem very distant if it were bright enough to be seen by an extragalactic observer (Eatough et al. 2013). Nonetheless, we note that of the five unambiguously localised FRBs, no source has a host-galaxy DM that is known to be significantly more than half its extragalactic DM (Tendulkar et al. 2017; Bannister et al. 2019; Prochaska & Zheng 2019; Ravi et al. 2019; Marcote et al. 2020).

If there were a radio source associated with M33 at 840 kpc, we can set an upper limit on its luminosity of $\nu L_\nu < 8.5 \times 10^{31}\,\mathrm{erg\,s^{-1}}$. At 1400 MHz, many supernova remnants (Chomiuk 2010) and HII regions (Paladini et al. 2009) would have been detectable if they were at the same distance as M33. M33 is known to have RGB stars stretching $\sim 2\,^\circ$ north of the core, nearly three times the radius of the classical disk (McConnachie et al. 2009, 2010), due to past interactions with M31. The northern part of M33 also has many HII regions (Relaño et al. 2013), but most are within 10 kpc of the core (30 arcminutes below FRB 191108). Therefore, while it is plausible that there would be stellar structure or star formation at the location of FRB 191108, we do not find evidence for a strong Faraday rotating plasma associated with M33. These facts, along with the arguments presented in Sect. 4.1, suggest the FRB RM arises in its host galaxy.

3.3 Time & frequency structure

We do not find evidence of temporal scattering in FRB 191108. Even though visually there appears to be slightly more power after the main peak of the FRB pulse profile than before it, the detected pulse width is consistent with intra-channel dispersion smearing and the sampling time of our instrument. We have also fit pulse width as a function of frequency and found the data to prefer dispersion smearing over scattering. The latter would result in a $\tau \propto \nu^{-4}$ relationship for a single-screen, whereas instrumental smearing between channels causes the width to scale as ν^{-3}, assuming dispersion smearing is larger than sampling time. We find the best-fit $\tau(\nu)$ power-law to be -2.9, implying that the pulse is temporally unresolved even at 275 μs. We also compared our pulse with simulation codes `simpulse`[3] and `injectfrb`[4], which generate realistically smeared FRBs and account for finite channelisation and temporal sampling. We simulated bursts with the same DM but varying intrinsic widths, assuming the same time and frequency resolution as ARTS, and fit their "observed" widths with the same pipeline that was used for the FRB. We found that the intrinsic width of FRB 191108 must be $\lesssim 80\,\mu$s.

In the top panel of Fig. 2, there is excess power after the primary pulse, and between 17 and 19 ms the PA appears non-random and consistent with the PA of the main pulse. Indeed, when the primary pulse is masked out, we find a 7.5 σ pulse whose best-fit width is 1 ms. This broader, weaker sub-pulse after the bright, narrow main pulse has been seen in other FRBs, for example the repeating FRB 180916.J0158+65 (see pulse *d* in Fig. 1 from Marcote et al. 2020) as well as the first repeater, FRB 121102 (see pulse *a* in Fig. 1 from Michilli et al. 2018).

As argued by Connor (2019), the observed widths of many FRBs are close to the instrumental smearing timescale, i.e. $\sim \sqrt{\tau^2_{\rm DM} + t^2_{\rm samp}}$, indicating that there may exist large numbers of narrow bursts that are missed by current search backends. When FRBs are coherently dedispersed or observed with high time/freq resolution, structure is often revealed on tens of microseconds timescales (Ravi et al. 2016; Farah et al. 2018; Hessels et al. 2019). FRB 191108 may therefore be an example of this population of narrow FRBs that are often missed without high time and frequency resolution backends—something Apertif has.

A least-squares power-law fit was applied to the Stokes I frequency spectrum of the FRB, yielding a power-law index of -1.6 ± 0.5. But like other FRBs, FRB 191108 is not well-described by a power-law. In the center and top of the band there is a factor of ~ 2 of excess power. This can be seen in the bottom panel of Fig. 2. Such bandedness has been seen in more extreme cases by ASKAP (Shannon et al. 2018), CHIME (CHIME/FRB Collaboration et al. 2019a), as well as in FRB 121102 (Hessels et al. 2019; Gourdji et al. 2019) and may prove to be a generic property of FRB spectra.

[3] https://github.com/kmsmith137/simpulse
[4] https://github.com/liamconnor/injectfrb

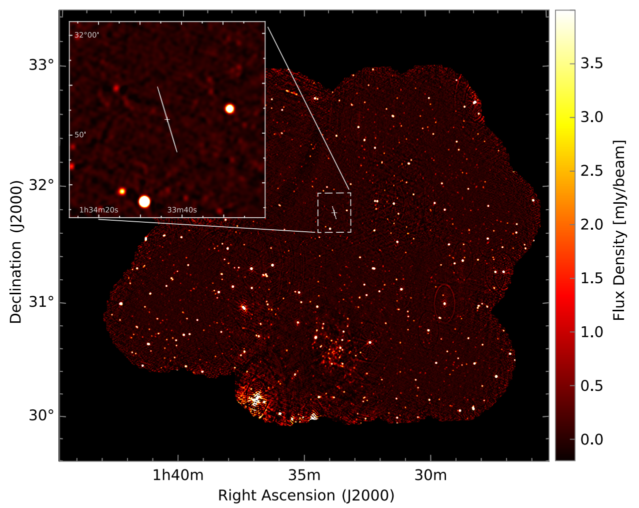

Figure 4: A mosaic from the Apertif imaging surveys combining 31 compound beams from two adjacent pointings around the localisation region. The mosaic has a synthesized beam of 31.6 arcsec × 31.6 arcsec. In the FRB localisation region, marked by the white ellipse, no persistent radio counterpart brighter than ~350 μJy (5 σ limit) was found.

3.4 M33 and M31 halos

The sky location of FRB 191108 is spatially separated by $1.20 \pm 0.05^\circ$ and $13.90 \pm 0.04^\circ$ from Local Group galaxies M33 and M31, respectively. As M33 is located at a distance of 840 kpc from the Milky Way, this translates to an impact parameter of 18 kpc to the M33 core. M31 is approximately 770 kpc away, meaning FRB 191108 came within roughly 185 kpc of Andromeda. Since they are relatively nearby, the circumgalactic medium (CGM) around the two galaxies, as well as the baryonic bridge between them, subtend a large angular size. We therefore expect the FRB to have traveled through both galaxies' CGM. Below we consider how these media might have contributed detectable propagation effects to the pulse signature of FRB 191108.

3.4.1 *Local Group DM contribution*

Prochaska & Zheng (2019) model the CGM of M31, which is large enough to engulf the CGM of M33, as it extends $\sim 30^\circ$. They use a modified Navarro–Frenk–White (NFW) profile and assume $M^{\rm M31}_{\rm halo} \approx 1.5 \times 10^{12}\,{\rm M}_\odot$ and $M^{\rm M33}_{\rm halo} \approx 5 \times 10^{11}\,{\rm M}_\odot$. Prochaska & Zheng also consider a 'Local Group Medium (LGM)', which models the total intra-group plasma. Using Fig. 9 in that paper, FRB 191108 would have an additional $\sim$40–60 pc cm^{-3} imparted by the halos of M33 and M31, but perhaps more depending on the nature of the intragroup plasma.

The hot gas in the Milky Way halo is also expected to contribute to the DMs of extragalactic objects. Prochaska & Zheng (2019) estimate a typical contribution of 50–80 pc cm^{-3}. Yamasaki & Totani (2019) use recent diffuse X-ray observations to model the halo DM, and account for the apparent directional dependence of emission measure (EM). The authors include a hot disk-like halo component as well as the standard spherically symmetric halo to calculate $\rm DM_{halo}$ as a function of Galactic longitude and latitude. Using their analytic prescription, we estimate the Milky Way halo contribution to be 30 ± 20 pc cm^{-3} in the direction of FRB 191108. **?** find a broader range of allowed values for the Galactic halo DM contribution than previous studies, but also favour smaller values. Combining the estimates of DM from the Milky Way ISM and halo, along with the plasma surrounding M33 and M31, the DM of FRB 191108 *beyond* the Local Group could be 380–480 pc cm^{-3}.

Using the approximate DM/redshift relation from Petroff et al. (2019),

$$\mathrm{DM} \approx 930\, z \quad \mathrm{pc\,cm^{-3}} \tag{3}$$

and subtracting off the expected Milky Way and Local Group DM contribution, the implied redshift upper limit on the source is 0.52.

ASKAP has also found an FRB that appears to pass through an intervening halo, coming within ~ 30 kpc of a massive foreground galaxy (Prochaska et al. 2019). This allowed the authors to place constraints on the net magnetization and turbulence in the foreground galaxy halo, due to the relatively low RM and dearth of scattering in FRB 181112. In our case, the high RM of FRB 191108 does not set a strong upper-limit on the halo magnetic field along the line of sight. Instead we suggest using the large number of polarised extragalactic objects behind M31 and M33 to constrain their CGM (see Fig. 6).

3.4.2 *CGM scattering & scintillation*

Recently, quasar absorption spectroscopy has been used to constrain CGM gas (Prochaska et al. 2014). Contrary to simple physical models of virialisation in massive dark matter halos, the absorption studies have found that most quasars that pass within ~ 150 kpc of a foreground galaxy indicate the existence of cool (10^4 K) gas embedded in a hot (10^6 K) CGM. It has been argued that gas in these environments is prone to fragmentation, leading to a 'cloudlet' model of the CGM in which sub-parsec cold gas clumps are distributed throughout the hot background medium (McCourt et al. 2018). Vedantham & Phinney (2019) investigated whether or not this cloudlet model of the CGM could impact FRBs.

The lensed geometric time delay is maximised when the foreground galaxy is halfway between the observer and the source. Given M33 is at a distance of just 840 kpc and the FRB emitting source is likely much farther away, we do not expect detectable temporal scattering from the intervening halo. Instead, we might expect to see frequency scintillation. NE2001 predicts a scintillation bandwidth of ≈ 1.8 MHz in the FRB direction (Cordes 2004), which is expected to occur if the FRB has not been significantly scatter broadened before entering the Galaxy. We compute the autocorrelation function of the FRB frequency spectrum and fit it with a Lorentzian function (Lorimer & Kramer 2012), finding a de-correlation bandwidth of $\Delta\nu \sim 40$ MHz, shown in Fig. 5. This appears to be dominated by the patches of increased brightness around 1370 MHz and 1500 MHz, which are approximately as wide as the best-fit de-correlation bandwidth. This is an order of magnitude larger than the expected Galactic scintillation bandwidth in the FRB direction.

To search for Galactic scintillation, we tried removing frequency modulation on scales above 20 MHz by subtracting a tenth-order polynomial fit from the data, allowing us to look for correlations at smaller $\Delta\nu$. We found positive correlation below a few MHz at the level of 5%, which is lower in amplitude than FRB 110523 (Masui et al. 2015), but roughly the same as the ACF found for FRB 180916.J0158+65 (Marcote et al. 2020). All are consistent with the decorrelation bandwidth from Galactic scintillation predicted by NE2001 at their respective frequencies.

If the $\Delta\nu \sim 40$ MHz frequency modulation were scintillation originating in the halo of M33, angular broadening would cause the FRB to no longer be a point source for Galactic scattering screens and we should not see correlations at 1−2 MHz scales. The angular broadening can be determined by noting $\tau \approx 1/2\pi\Delta\nu = 4$ ns. Assuming the FRB is emitted from a much greater distance than M33, the broadening is given by (Thompson et al. 2017),

$$\theta \approx \sqrt{\frac{2\,c\,\tau}{d_{\mathrm{M33}}}} \approx 2\,\mu\text{arcsecond}. \tag{4}$$

If the origin of the frequency modulation of FRB 191108 is indeed interference from a scattering screen near M33 and not intrinsic to the source, Galactic scintillation would be quenched. Scintillation tends to only occur for sources smaller than 0.1 arcseconds at 1 GHz, because extragalactic sources will not scintillate if their angular size is significantly greater than the Fresnel scale of the scattering screen (Dennett-Thorpe & de Bruyn 2002). This is why so few quasars scintillate in the ISM but pulsars do, and why stars scintillate in our atmosphere but the planets do not. These arguments against the frequency modulations originating in scintillation near the M33 halo are in line with other FRBs, which often show banded structure over 10s or 100s of MHz.

Table 1. FRB 191108 parameters. † are values that have been optimised post real-time detection, chosen to maximise S/N in the the case of width and DM. Our localisation region is an ellipse whose semi-major and semi-minor axes do not correspond to RA and Dec, so we do not quote uncertainty on those values. For the true sky localisation parameterisation, see Sect. 3.2. The width listed here is dominated by intra-channel dispersion smearing, but we set an upper-limit on its intrinsic width at 80 μs.

Date	2019 November 8
UTC[(a)]	19:48:50.471
MJD[(b)]	58795.830818389
RA (J2000)	01h33m47s
Dec (J2000)	+31d51m30s
DM†	588.1±0.1 pc cm^{-3}
RM	474±3 rad m^{-2}
Width† (1370 MHz)	340±20 μs
Flux density	27 Jy
S/N$_{\mathrm{det}}$	60
S/N$^{\dagger}_{\mathrm{opt}}$	103
DM$_{\mathrm{MW}}$ (YMW16/NE2001)	43 / 52 pc cm^{-3}
RM$_{\mathrm{MW}}$	−50 rad m^{-2}
z_{max}	0.52

[(a)] At 1370 MHz.
[(b)] At the solar system barycenter after removal of the DM delay.

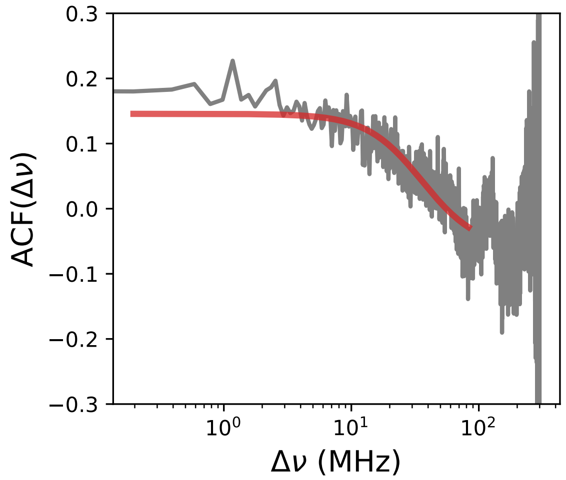

Figure 5: The autocorrelation function of the FRB spectrum, with a best-fit Lorenzian overplotted in red whose de-correlation bandwidth is 40 MHz.

4 DISCUSSION

4.1 Rotation measure origin

The observed RM of an FRB can be broken down into several components between the observer and source,

$$\mathrm{RM_{obs}} = \mathrm{RM_{MW}} + \mathrm{RM_{IGM}} + \mathrm{RM_{host}}, \tag{5}$$

where $\mathrm{RM_{MW}}$ is the foreground RM from the Galaxy, $\mathrm{RM_{IGM}}$ is from the intergalactic medium, and $\mathrm{RM_{host}}$ comes from the host galaxy ISM and the region near the FRB progenitor. In the case of FRB 191108, we might also include $\mathrm{RM_{LG}}$, the contribution from the Local Group. This is the contribution of the galactic halos of M33 (Triangulum) and M31 (Andromeda), and the broader shared plasma linking the two nearby galaxies with the Milky Way. With $\mathrm{RM_{obs}}$=+474 ± 3 rad m^{-2} and an expected Milky Way foreground of $\mathrm{RM_{MW}} \approx -50$ rad m^{-2} (Fig. 6 provides an idea of the spatial scatter of this value) (Oppermann et al. 2015), the estimated extragalactic contribution is approximately 525 rad m^{-2}. Such a large extragalactic RM is not expected from the IGM, as it would require ordered μG magnetic fields over gigaparsec scales to achieve 10^{2-3} rad m^{-2} for typical FRB redshifts. No intergalactic magnetic fields have been detected, but they are expected to be roughly nG in strength.

We consider the possibility that the ionised material surrounding M33/M31 could contribute all the required magnetised plasma to account for the RM of the FRB, but do not find this compelling for the following reason. By taking the catalogue of 41632 extragalactic RMs from Oppermann et al. (2012), we identify 93 objects that pass within 5° of M33, roughly the angular radius of the expected 75 kpc halo. 93% of these sources have RMs between −15 and −90 rad m^{-2}—likely dominated by the Milky Way foreground like most polarised extragalactic sources—and none is larger in magnitude than 100 rad m^{-2}. In Fig. 6 we plot the distribution of extragalactic RMs near the Local Group on the sky to demonstrate the extent to which FRB 191108 is an outlier. Therefore, unless the source has a very unusual sight-line and travels through a dense magnetoionic region in the M33/M31 halo with the opposite magnetic field sign, the absence of strong Faraday rotation in other extragalactic polarised sources behind M33 suggests the FRB RM is imparted elsewhere. The dataset plotted in Fig. 6 could still be a useful probe of CGM magnetic fields in its own right: the black points in the left panel that have a low impact parameter with M31 show a small gradient such that their amplitude increases towards smaller angular separations. Whether this is due to structure in the Galactic foreground Faraday field or in the M31 halo could be teased out with a Galactic DM map.

Given we do not expect the large RM of the FRB to be dominated by the Milky Way, M33, or the IGM, it is likely that the magnetised plasma is in the host galaxy. Using the estimated maximum redshift implied by the extragalactic DM, of $z \approx 0.52$, and noting that the local RM will be a factor of $(1 + z)^2$ larger than the observed RM due to cosmological redshift, $\mathrm{RM_{host}}$ could be of order 10^3 rad m^{-2}. Even if the host galaxy contributes significantly to the extragalactic DM and the FRB is much closer than the redshift implied by Eq. 3, the RM would still be much larger than that expected from the ISM of a Milky Way-like galaxy, unless observed very close to edge-on.

FRBs are now known to be located in a range of environments spanning different galaxy types. While there exist examples of polarised FRBs without significant Faraday Rotation (Ravi et al. 2016; Petroff et al. 2017), now including a repeater (Fonseca et al. 2020), several sources appear to pass through regions of highly-magnetised plasma. The first was FRB 110523, which was detected with the Green Bank Telescope. It had an RM of −186 rad m^{-2}. Like the Apertif-discovered FRB 191108, this is larger than expected from the Milky Way and the IGM (Masui et al. 2015). The authors argued that its high RM and scattering properties suggested a dense magnetised environment local to the source. The FRB with the highest published DM, FRB 160102, had an RM of −220 rad m^{-2} (Caleb et al. 2018); its local RM could be as large as −2400 rad m^{-2} if a significant portion of the DM comes from the IGM. During Breakthrough Listen observations on the Parkes telescope, FRB 180301 was detected and full-polarisation data was preserved (Price et al. 2019). They report an RM of -3163 ± 20 rad m^{-2}, though the patchiness of their frequency spectrum causes the authors to question their Faraday rotation fit. CHIME has found a repeating FRB whose RM exceeds the Galactic foreground by two orders of magnitude, with RM=-499.8 ± 0.7 rad m^{-2} (Fonseca et al. 2020). Finally, FRB 121102 has an RM of $\sim 10^5$ rad m^{-2} and is spatially coincident with a bright, compact radio source (Michilli et al. 2018). This is larger than even the Galactic center magnetar, PSR J1745−2900, with RM $\sim 7 \times 10^4$ rad m^{-2} (Eatough et al. 2013). Both FRB 121102 and PSR J1745−2900 have been seen to exhibit significant RM variation over month to year timescales (Desvignes et al. 2018).

The analogy between FRB 121102 and the Galactic center magnetar may extend beyond just phenomenological similarities. If the persistent radio source coincident with FRB 121102 is similar to a low-luminosity active galactic nucleus (LLAGN), then that system may be another example of a circumnuclear magnetar, a scenario that has been proposed as a progenitor theory of FRBs (Pen & Connor 2015). Alternatively, the radio nebula could correspond to a supernova remnant, magnetar wind nebula, or HII region. Such local environments have been invoked as a way to provide local RM, DM, and scattering (Connor et al. 2016a; Piro 2016; Murase et al. 2016; Piro & Gaensler 2018; Margalit & Metzger 2018). In each of these cases, it is difficult to predict the distribution of observed RMs, but it is likely that the distribution would be broad. For example, in the circumnuclear magnetar model, the FRB RM is a strong function of its distance from the massive black hole. In young magnetar or supernova remnant models, the RM is expected to change with time, and the value depends on when in the progenitor life cycle the FRB was observed. Thus, moderately large RMs like those of FRB 191108, FRB 110523 (Masui et al. 2015), and FRB 160102 (Caleb et al. 2018) may come from a similar environment to FRB 121102.

4.2 Repetition constraints

Given the extreme local environment of FRB 121102 and its anomalously high repetition rate, it may be asked if frequent repeaters are more likely to live near dense magnetised plasma. CHIME recently discovered a repeating FRB whose RM is −499.8 ± 0.7 rad m^{-2}, which is roughly two orders of magnitude larger than the expected Milky Way contribution in that direction (Fonseca et al. 2020). But Fonseca et al. (2020) also report a repeater with RM=−20 ± 1 rad m^{-2}, and most of the RM=−114.6 ± 0.6 rad m^{-2} from another CHIME repeating source, FRB 180916.J0158+65, is thought to be from the Milky Way (CHIME/FRB Collaboration et al. 2019c).

We observed the field of FRB 191108 for 120 hours between July 2019 and December 2019 with no repeat detections. Assuming repetition statistics described by a homogeneous Poisson process, this gives a 3 σ upper-limit on the repeat rate of 3×10^{-2} per hour.

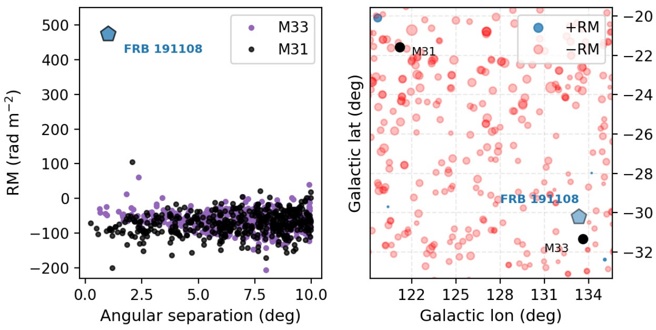

Figure 6: The RMs of extragalactic sources in the direction of the Local Group galaxies M33 and M31. The left panel shows RM vs. angular separation for both M33 (purple) and M31 (black), as well as the FRB which is an outlier both in amplitude and sign. The right panel shows extragalactic sources, where the size of the marker indicates |RM| and the colour encodes its sign.

We caution, however, that the assumption of stationarity is known to not be valid for some FRBs, which show time-variability in their repetition rate (Spitler et al. 2016; Oppermann et al. 2018; Gourdji et al. 2019) thereby increasing the probability of seeing zero repeat bursts during follow up (Connor et al. 2016b).

The source position is slightly outside the area around M33 that Mikhailov & van Leeuwen (2016) searched for FRBs and pulsars with LOFAR. But using the LOFAR Transient Buffer Boards (TBBs), FRB 191108 will be observed simultaneously with Apertif and LOFAR. The TBBs allow LOFAR to save voltage data across multiple stations between 100–200 MHz and search for emission over a decade in frequency.

We plan to continue follow-up efforts on the same field, which we can do commensurate with our full-FoV blind FRB search. The source is currently localised to an ellipse with semi-minor and semi-major axes of 2.5 $''$ and 3.5 $'$, respectively, as described in Sect. 3.2. If we detect FRB 191108 again at a different hour angle than the initial detection, we will have several arcsecond localisation in both directions, because the TABs rotate as a function of parallactic angle.

5 CONCLUSIONS

We have reported the detection of a bright, highly Faraday rotated FRB in the direction of Local Group galaxy M33 using Apertif. By combining multibeam information from the Apertif PAF and the tied-array beams, we were able to localise FRB 191108 to a narrow ellipse with a semi-major axis of 5 $'$, a semi-minor of axis 2.5 $''$, and a position angle 19.5° East of North. The impact parameter with M33 is just 18 kpc, roughly the diameter of that galaxy's disk. The RM of +474±3 rad m^{-2} is one of the largest of any published value and is an order of magnitude larger than the expected contribution from the Milky Way, the IGM, and the halos of M33/M31. The most plausible location of the magnetised plasma is therefore a dense region near the FRB-emitting source itself.

While the shared plasma in the halos of M33 and M31 would have contributed to the DM of the FRB, we deem it unlikely that the nearby plasma significantly scattered, Faraday rotated the burst, or caused scintillation. The FRB field was observed for a total of 120 hours in the second half of 2019 with no repeat bursts detected. Looking forward, we plan to continue monitoring FRB 191108 to search for repetition, as a connection between FRB repetition and local environment remains an open question in the field. Detecting another burst from the source at a different hour angle will also allow for ~ arcsecond localisation in two dimensions, as the narrow tied-array beams rotate on the sky with parallactic angle. We plan to observe the FRB simultaneously with Apertif at 1370 MHz and LOFAR at 100–200 MHz, using the latter's voltage-saving TBBs.

ACKNOWLEDGEMENTS

We thank Dan Stinebring, Jason Hessels, and Monica Relano Pastor for helpful conversations. This research was supported by the European Research Council under the European Union's Seventh Framework Programme (FP/2007-2013)/ERC Grant Agreement No. 617199 ('ALERT'), and by Vici research programme 'ARGO' with project number 639.043.815, financed by the Dutch Research Council (NWO). Instrumentation development was supported by NWO (grant 614.061.613 'ARTS') and the Netherlands Research School for Astronomy ('NOVA4-ARTS' and 'NOVA-NW3'). EP acknowledges funding from an NWO Veni Fellowship. AS and DV acknowledge support from the Netherlands eScience Center (NLeSC) under grant ASDI.15.406. SMS acknowledges support from the Netherlands Research School for Astronomy (NOVA4-ARTS), and was supported by the National Aeronautics and Space Administration (NASA) under grant number NNX17AL74G issued through the NNH16ZDA001N Astrophysics Data Analysis Program (ADAP). EAKA is supported by the WISE research programme, which is financed by NWO.

REFERENCES

Adams E. A. K., van Leeuwen J., 2019, Nature Astronomy, 3, 188
Bannister K. W., et al., 2019, Science, 365, 565
Bassa C. G., et al., 2017, ApJ, 843, L8
CHIME/FRB Collaboration et al., 2019a, Nature, 566, 230
CHIME/FRB Collaboration et al., 2019b, Nature, 566, 235
CHIME/FRB Collaboration et al., 2019c, ApJ, 885, L24
Caleb M., et al., 2018, MNRAS, 478, 2046
Chatterjee S., et al., 2017, Nature, 541, 58
Chomiuk L., 2010, in American Astronomical Society Meeting Abstracts #215. p. 356.03
Connor L., 2019, MNRAS, 487, 5753
Connor L., van Leeuwen J., 2018, AJ, 156, 256
Connor L., Sievers J., Pen U.-L., 2016a, MNRAS, 458, L19
Connor L., Pen U.-L., Oppermann N., 2016b, MNRAS, 458, L89
Cordes J. M., 2004, NE2001: A New Model for the Galactic Electron Density and its Fluctuations. p. 211
Cordes J. M., Chatterjee S., 2019, ARA&A, 57, 417
Dennett-Thorpe J., de Bruyn A. G., 2002, Nature, 415, 57
Desvignes G., et al., 2018, ApJ, 852, L12
Eatough R. P., et al., 2013, Nature, 501, 391
Eftekhari T., Berger E., 2017, ApJ, 849, 162
Eftekhari T., Berger E., Williams P. K. G., Blanchard P. K., 2018, ApJ, 860, 73
Eichler D., 2017, ApJ, 850, 159
Farah W., et al., 2018, MNRAS, 478, 1209
Fonseca E., et al., 2020, arXiv e-prints, p. arXiv:2001.03595
Gajjar V., et al., 2018, ApJ, 863, 2
Gourdji K., Michilli D., Spitler L. G., Hessels J. W. T., Seymour A., Cordes J. M., Chatterjee S., 2019, ApJ, 877, L19
Hessels J. W. T., et al., 2019, ApJ, 876, L23
Kumar P., et al., 2019, The Astrophysical Journal, 887, L30
Lorimer D. R., Kramer M., 2012, Handbook of Pulsar Astronomy

Lorimer D. R., Bailes M., McLaughlin M. A., Narkevic D. J., Crawford F., 2007, Science, 318, 777
Maan Y., van Leeuwen J., 2017, IEEE Proc. URSI GASS,
Marcote B., et al., 2017, ApJ, 834, L8
Marcote B., et al., 2020, arXiv e-prints, p. arXiv:2001.02222
Margalit B., Metzger B. D., 2018, ApJ, 868, L4
Masui K., et al., 2015, Nature, 528, 523
McConnachie A. W., et al., 2009, Nature, 461, 66
McConnachie A. W., Ferguson A. M. N., Irwin M. J., Dubinski J., Widrow L. M., Dotter A., Ibata R., Lewis G. F., 2010, ApJ, 723, 1038
McCourt M., Oh S. P., O'Leary R., Madigan A.-M., 2018, MNRAS, 473, 5407
McQuinn M., 2014, ApJ, 780, L33
Michilli D., et al., 2018, Nature, 553, 182
Mikhailov K., van Leeuwen J., 2016, A&A, 593, A21
Muñoz J. B., Kovetz E. D., Dai L., Kamionkowski M., 2016, Phys. Rev. Lett., 117, 091301
Murase K., Kashiyama K., Mészáros P., 2016, MNRAS, 461, 1498
Oosterloo T., Verheijen M., van Cappellen W., 2010, in "ISKAF2010 Science Meeting", Van Leeuwen, Morganti, Serra (Eds.). (`arXiv:1007.5141`)
Oppermann N., et al., 2012, A&A, 542, A93
Oppermann N., et al., 2015, A&A, 575, A118
Oppermann N., Yu H.-R., Pen U.-L., 2018, MNRAS, 475, 5109
Paladini R., DeZotti G., Noriega-Crespo A., Carey S. J., 2009, The Astrophysical Journal, 702, 1036
Pen U.-L., Connor L., 2015, ApJ, 807, 179
Petroff E., et al., 2016, Publ. Astron. Soc. Australia, 33, e045
Petroff E., et al., 2017, Monthly Notices of the Royal Astronomical Society, 469, 4465
Petroff E., Hessels J. W. T., Lorimer D. R., 2019, A&ARv, 27, 4
Piro A. L., 2016, ApJ, 824, L32
Piro A. L., Gaensler B. M., 2018, ApJ, 861, 150
Price D. C., et al., 2019, MNRAS, 486, 3636
Prochaska J. X., Zheng Y., 2019, MNRAS, 485, 648
Prochaska J. X., Lau M. W., Hennawi J. F., 2014, ApJ, 796, 140
Prochaska J. X., et al., 2019, Science, 365, aay0073
Ravi V., et al., 2016, Science, 354, 1249
Ravi V., et al., 2019, Nature, 572, 352
Relaño M., et al., 2013, Astronomy and Astrophysics, 552
Sclocco A., Van Nieuwpoort R., Bal H. E., 2014, in Exascale Radio Astronomy.
Sclocco A., van Leeuwen J., Bal H. E., van Nieuwpoort R. V., 2016, Astronomy and Computing, 14, 1
Sclocco A., Vohl D., van Nieuwpoort R. V., 2020, arXiv e-prints, p. arXiv:2001.03389
Shannon R. M., et al., 2018, Nature, 562, 386
Spitler L. G., et al., 2014, ApJ, 790, 101
Spitler L. G., et al., 2016, Nature, 531, 202
Tendulkar S. P., et al., 2017, ApJ, 834, L7
Thompson A. R., Moran J. M., Swenson George W. J., 2017, Interferometry and Synthesis in Radio Astronomy, 3rd Edition, doi:10.1007/978-3-319-44431-4.
Vedantham H. K., Phinney E. S., 2019, MNRAS, 483, 971
Walters A., Weltman A., Gaensler B. M., Ma Y.-Z., Witzemann A., 2018, ApJ, 856, 65
Yamasaki S., Totani T., 2019, arXiv e-prints, p. arXiv:1909.00849
Yao J. M., Manchester R. N., Wang N., 2017, ApJ, 835, 29
York D. G., et al., 2000, AJ, 120, 1579
van Leeuwen J., 2014, in Wozniak P. R., Graham M. J., Mahabal A. A., Seaman R., eds, "The Third Hot-wiring the Transient Universe Workshop". p. 79
van Leeuwen J., Kooistra E., Connor L., Maan Y., Oostrum L., et al. 2020, in prep